Investigation of the redox centres of periplasmic selenate reductase from Thauera selenatis by EPR spectroscopy

Elizabeth J Dridge, Carys A Watts, Brian J Jepson, Kirsty Line, Joanne M Santini, David J Richardson, Clive S Butler

Biochemical Journal Immediate Publication. Published on 10 Aug 2007 as manuscript BJ20070669

Investigation of the redox centres of selenate reductase from *Thauera selenatis* by electron paramagnetic resonance spectroscopy

Elizabeth J. DRIDGE[1,2†], Carys A. WATTS[2†], Brian J.N. JEPSON[3], Kirsty LINE[1], Joanne M. SANTINI[4], David J. RICHARDSON[3] and Clive S. BUTLER[1*]

[1]School of Biosciences, Centre for Biocatalysis, University of Exeter, Stocker Road, Exeter EX4 4QD, UK

[2]Institute for Cell and Molecular Biosciences, University of Newcastle, Newcastle upon Tyne NE2 4HH, UK

[3]School of Biological Sciences, University of East Anglia, Norwich NR4 7TJ, UK

[4]Department of Biology, UCL, Gower Street, London WC1E 6BT, UK

Short title: The redox centres of selenate reductase probed by EPR spectroscopy

Key words: selenate reductase; molybdoenzyme; EPR spectroscopy; iron-sulfur clusters

Abbreviations: MGD, molybdenum guanine dinucleotide; SER, periplasmic selenate reductase; NAR, membrane-bound nitrate reductase; NAP, periplasmic nitrate reductase; EBDH, ethylbenzene dehydrogenase; DMSDH, dimethyl sulfide dehydrogenase; DMSOR, dimethylsulfoxide reductase; FDH, formate dehydrogenase; FeS/FS0-5, iron-sulfur clusters; Tat, twin-arginine translocation.

Footnote: [†]These authors contributed equally to this work

*Correspondence:
Dr Clive S. Butler
School of Biosciences
Centre for Biocatalysis
University of Exeter
Stocker Road
Exeter EX4 4QD

Tel: 01392 264675
Fax: 01392 263434
E-mail: c.s.butler@exeter.ac.uk

Biochemical Journal Immediate Publication. Published on 10 Aug 2007 as manuscript BJ20070669

Synopsis

Selenate reductase (SerABC) from *Thauera selenatis* is classified as a member of the Tat-translocated (Type II) molybdo-enzymes and comprises three subunits each containing redox cofactors. Variable temperature X-band electron paramagnetic resonance (EPR) spectra of the purified selenate reductase complex showed features attributable to centres $[3Fe\text{-}4S]^{1+}$, $[4Fe\text{-}4S]^{1+}$, Mo(V) and haem-*b*. EPR monitored redox-potentiometric titration of SerABC complex (hetero-trimetric complex of $\alpha\beta\gamma$ subunits) revealed that the [3Fe-4S] cluster (FS4) titrated as $n = 1$ Nernstian component with a mid-point redox potential (E_m) of +118 ± 10 mV mV for the $[3Fe\text{-}4S]^{+1/0}$ couple. A $[4Fe\text{-}4S]^{1+}$ cluster EPR signal developed over a range of potentials between 300 and -200 mV and was best fitted to two sequential Nernstian $n = 1$ curves with midpoint redox potentials of +183 ± 10 mV (FS1) and -51 ± 10 mV (FS3) for the two $[4Fe\text{-}4S]^{1+/2+}$ cluster couples. Upon further reduction, the observed signal intensity of the $[4Fe\text{-}4S]^{1+}$ cluster decreases. This change in intensity can again be fitted to an n=1 Nernstian component with a mid-point potential of E_m~-356 mV (FS2). It is considered likely that at low redox potential E_m<-300 mV, the remaining oxidised cluster is reduced (S=1/2) and strongly spin-couples to a neighbouring $[4Fe\text{-}4S]^{1+}$ cluster rendering both centres EPR silent. The involvement of both [3Fe-4S] and [4Fe-4S] clusters in electron transfer to the active site of selenate reductase was demonstrated by the re-oxidation of the clusters under anaerobic selenate turnover conditions. Attempts to detect a high-spin [4Fe-4S] cluster (FS0) in SerA at low temperature (5 K) and high power (100 mW) were unsuccessful. The Mo(V) EPR recorded at 60 K, in samples poised at pH 6.0, displays principal g values of g_3~1.999, g_2~1.996 and g_1~1.965 (g_{av} 1.9867). The dominant features at g_2 and g_3 are not split, but hyperfine splitting is observed in the g_1 region of the spectrum and can be best simulated as arising from a single proton with a coupling constant of A_1 (^{1}H) = 1.014 [mT]. The presence of the haem-*b* moiety in SerC was demonstrated by the detection of a signal at g~3.33 and is consistent with haem co-ordinated by methionine and lysine axial ligands. The combined evidence from EPR analysis and sequence alignments supports the assignment of the periplasmic selenate reductase as a member of the Type II molybdo-enzymes and provides the first spectro-potentiometric insight into an enzyme that catalyses a key reductive reaction in the biogeochemical selenium cycle.

Introduction

The microbial reduction of selenium oxyanions is a key process in the transformation of selenium in the biosphere [1,2]. The oxidised and bio-available forms of selenium (selenate (SeO_4^{2-}) and selenite (SeO_3^{2-})) can be utilised as respiratory substrates by some bacteria, resulting in their reduction to elemental selenium (Se^0). Elemental selenium readily precipitates and is largely unavailable for assimilation into seleno-proteins [3]. Whilst a number of organisms respire selenium oxyanions, little is known about the biochemistry of the selenate reductive process. To date, the purification of only two selenate reductases has been reported [4,5]. The enzyme isolated from *Enterobacter cloacae* SLD1a-1 is membrane-bound and comprises three subunits of ~100 kDa, ~55 kDa and ~36 kDa, with the 100 kDa protein functioning as the catalytic subunit [5]. Although it was reported that the enzyme complex contained molybdenum, haem and non-haem iron, low protein yields have subsequently prevented any detailed spectroscopic characterisation of these redox cofactors [5]. The dissimilatory selenate reductase isolated from *Thauera selenatis* [6], in contrast, is a soluble periplasmic enzyme and is much more abundantly produced than the membrane-bound enzyme in *E. cloacae* SLD1a-1. The periplasmic enzyme (termed SER) also comprises three subunits, SerA (96 kDa), SerB (40 kDa) and SerC (23 kDa) and catalyses the two electron reduction of selenate to selenite as shown in reaction (1).

$$SeO_4^{2-} + 2e^- + 2H^+ \rightarrow SeO_3^{2-} + H_2O \qquad (1)$$

The SerA subunit has an N-terminal cysteine-rich motif ($HX_3CX_3CX_{34}C$), probably co-ordinating a [4Fe-4S] cluster and also contains the molybdenum (Mo) active site in the form of the molybdopterin guanine dinucleotide (*bis*-MGD) cofactor [4,7,8]. The SerB subunit also has four cysteine rich motifs, which again suggest the presence of a number of iron-sulfur clusters. The SerABC complex also contains a *b*-type cytochrome as shown by absorption spectroscopy [4], and this is presumed to be co-ordinated to the SerC subunit. The selenate reductase shows substrate selectivity and does not reduce nitrate, arsenate or sulphate, but does reduce chlorate (Bydder S and Santini JM, unpublished results). Amino acid sequence alignment of SerA with other molybdenum containing enzymes has shown that it is closely related to the Type-II molydo-proteins [9], a group that also includes the well characterised respiratory membrane-bound nitrate reductase NAR [10,11]. The highly conserved aspartate residue, shown to co-ordinate the Mo in NAR X-ray structures [12,13] is also conserved in

SerA. However, unlike the bacterial membrane-bound nitrate reductase (NarG), the selenate reductase SerA component has a leader sequence that targets the protein complex via the Tat (twin arginine translocase) apparatus to the periplasmic (potential positive, ψ^+) side of the membrane [14,15] and as such places selenate reductase as a member of a distinct subgroup of Tat-translocated D-group (Type II) molybdo-enzymes, that also includes; chlorate reductase (*Ideonella dechloratans* [16]), dimethyl sulfide dehydrogenase (*Rhodovulum sulfidophilum* [17]), perchlorate reductase (*Dechloromonas* species [18]) and ethylbenzene dehydrogenase (*Aromatoleum aromaticum* [19,20]). A number of putative enzyme complexes that are predicted to be unusual Tat-dependent nitrate reductases (pNAR) [21,22] have recently been identified in some archaeal genomes, and are also included in this Type II group [11]. Due to the relatively recent identification of this unusual sub-group of molybdo-enzymes, few spectroscopic studies of their redox centres have been reported, with the notable exception of the detailed study by McEwan and co-workers on the dimethyl sulfide dehydrogenase from *Rhodovulum sulfidophilum* [17]. Consequently, in the present work we have undertaken the first EPR spectroscopic analysis of the SerABC complex from *T. selenatis*, and probed the centres under oxidised, reduced and turnover conditions. Signals attributed to FeS clusters, haem-*b* and the Mo centre are reported and the assignment of these signals is discussed in relation to the recent crystal structure of ethylbenzene dehydrogenase (EBDH) [20].

Experimental

Growth of T. selenatis and production of periplasmic fractions.

T. selenatis was grown anaerobically at 30°C in mineral salts medium [6] containing yeast extract (0.1%), selenate (10 mM) and acetate (10 mM) in 10 litre batch cultures. Cultures were harvested during late log phase (after 16-18 hrs growth) at A_{600} 0.6-0.7 and spheroplasts were prepared as described previously [4]. The spheroplasts were removed by centrifugation (25,000 x *g*, 20 minutes) and the supernatant containing periplasm was retained.

The purification of the selenate reductase SerABC complex.

Selenate reductase was concentrated by ammonium sulphate precipitation (50-80%) as described previously [4]. After centrifugation (25,000 x *g*, 20 minutes), the precipitated proteins were suspended in 50 mM PIPES buffer pH 6.0, containing 1 M $(NH_4)_2SO_4$. The solution was directly loaded onto a Phenyl-Sepharose high performance hydrophobic interaction column, which had been equilibrated with 1M PIPES buffer pH 6.0, containing 1 M

$(NH_4)_2SO_4$. All chromatography procedures were performed at room temperature. Protein concentration was monitored by measuring the absorbance at 280 nm. After washing the column with one volume of PIPES buffer containing 1 M $(NH_4)_2SO_4$, the selenate reductase was eluted from the column with a 1-0 M $(NH_4)_2SO_4$ gradient in PIPES buffer. Following elution, fractions were assayed for selenate reductase activity using a viologen-based anaerobic microtitre plate assay [23], and those showing selenate reductase activity were pooled and concentrated using a 30 kDa cut-off Amicon ultrafiltration cell. The resulting fraction was loaded onto a Superdex 200 gel filtration column (Amersham) that had been equilibrated with two column volumes of 50mM PIPES (pH 6.0). The selenate reductase was eluted in the same buffer, with the fractions being assayed for selenate reductase activity as before, and those containing the activity were concentrated using a 30 kDa cut-off Vivaspin centrifugal concentrator and stored at -80°C. Purity was determined by SDS-PAGE. N-terminal sequence was performed as described previously [5] using the Molecular Biology Facility, University of Newcastle. In order to determine the metal (Fe and Mo) content of the purified selenate reductase, samples were analysed by inductively coupled plasma mass spectroscopy (ICPMS). Standards of Fe and Mo were prepared at the following concentrations 1, 5, 10, 25, 50 and 100 ppb. All samples and standards were treated with 6.5% nitric acid and analysed using a thermo X-series ICP-MS spectrometer in accordance with manufacturer's instructions.

Electron paramagnetic resonance spectroscopy

All EPR spectra were measured using a Bruker EMX spectrometer (X-band 9.38 GHz) equipped with an ER4112HV liquid helium flow cryostat system. Samples were prepared as detailed in the appropriate figure legends. FeS EPR spectra were recorded at a range of temperatures (5-25 K) and microwave powers (2-100 mW) at 9.38 GHz microwave frequency and 0.5 mT field modulation amplitude. Mo(V) EPR spectra were recorded at 60K, *ca*. 9.38 GHz microwave frequency, 2 mW microwave power and 0.5 mT field modulation amplitude. Spin concentration of samples was determined from integrations of their EPR absorption spectra by comparison to those of a 2 mM Cu^{II}-EDTA standard [24,25]. EPR monitored redox potentiometric titrations were performed as described previously [26]. Spectral simulations were carried out using WINEPR Simfonia Version 1.25 (Bruker). Where simulations are presented, experimental and simulated spectra are aligned with a magnetic field range corresponding to a microwave frequency of 9.3800 GHz.

Homology modelling

Homology modelling was carried out using the homology tools in the software package MOE™. The sequence of *T. selenatis* SerB was aligned and modelled against the structure of EBDH β-subunit from *A. aromaticum* (PDB - 2IVF B [20]). An ensemble of 30 intermediate models was created and the best intermediate model minimised using the CHARM22 force field to an RMS gradient of 0.01. The quality of the model was assessed by PROCHECK [27,28]. Molecular pictures were created using PyMol [29].

Results

EPR studies of the iron-sulfur clusters

Selenate reductase purifies as a three subunit complex (Figure 1 inset) and metal analysis has confirmed the presence of 24 ± 2 mol Fe and 0.5 ± 0.1 mol Mo per mol enzyme. Further purification to achieve homogeneity has resulted in a significant loss of activity and a concomitant decrease in the Mo content, consequently, the spectroscopic analysis presented here has been performed on a sample considered to be >80% pure. The only significant contaminant present is a protein of molecular mass ~28 kDa which we have confirmed by N-terminal sequence analysis to be uridine phosphorylase, and as such co-ordinates no EPR detectable clusters [30]. The variable temperature X-band (9.38 GHz) EPR spectra of as prepared "resting" SerABC (Figure 1) at 10K was dominated by a large signal centered at g_{av}~2.01, a small isotropic signal at g~4.3 and a feature at g~3.33 (Figure 1). The signal at g~4.3 is typical of that routinely observed for adventitious high-spin Fe^{III}. The line-shape of the large signal at g_{av}~2.01 is, in general, similar to that observed from proteins containing an oxidised (S=1/2) $[3Fe\text{-}4S]^{1+}$ cluster; notably the signal displays a low-field sharp positive peak followed by a less intense broad negative tail to high field [31]. The temperature dependence of the signal (Figure 2) shows that the signal broadens rapidly above 15K, such that at 20K the signal is barely detectable. The power dependence of the signal displays a $P_{1/2}$ ~ 50 mW at 10K (data not shown). Simulation of the spectrum recorded at 10K gives principal g values of g_1~1.991, g_2~2.004 and g_3~2.026 (g_{av}=2.007) (Figure 2). Assuming a ground state of spin S=1/2, double integration of the signal recorded under non-saturating conditions, when compared to a Cu^{II}-EDTA standard, yields a spin concentration representing a population of ~0.9 [3Fe-4S] clusters per SerABC unit. Upon reduction of the sample by the addition of excess sodium dithionite the signal at g_{av}~2.01 is no longer detectable and is now replaced by a number of features resolvable in the g~2 region (Figure 3). The principal signal (see

Biochemical Journal Immediate Publication. Published on 10 Aug 2007 as manuscript BJ20070669

simulation) with g values $g_{1,2}$~1.882 and g_3~2.026 (g_{av}~1.930) can be best described as an axial signal. It again shows temperature dependence and is no longer detectable at 40K, and as such is indicative of a $[4Fe\text{-}4S]^{2+}$ cluster rather than a HIPIP-type $[4Fe\text{-}4S]^{3+}$ or a reduced $[2Fe\text{-}2S]^{1+}$ cluster, which are often detected at temperatures up to 60 K or higher [31]. Power saturation studies (data not shown) demonstrate that this signal is difficult to saturate within the available power range ($P_{1/2}$ > 100 mW at 10K). This observed behaviour is consistent with other studies of [4Fe-4S] clusters in related enzymes. The signal shows resemblance to the axial signal observed for the minor conformation of the FS1 cluster in nitrate reductase NarH (Table 1). Since the g_{av} value (1.930) is less than g_e (2.00232), the electronic structure of the [4Fe-4S] cluster is more likely to be $[4Fe\text{-}4S]^{1+}$ than $[4Fe\text{-}4S]^{3+}$ [32] and is again in agreement with the observed temperature dependence. Assuming a ground state of spin S=1/2, double integration of the $[4Fe\text{-}4S]^{1+}$ signal, when compared to a Cu^{II}-EDTA standard, yielded a spin concentration representing a population of ~0.5 [4Fe-4S] clusters per SerABC unit. An additional signal is also observed at g~1.999, but is not subject to the same temperature dependence and can probably be assigned to the g_3 feature of the Mo(V) species (see below). Also, upon reduction, a number of low intensity broad resonances are observed in the g~1.96 region which probably arise due to spin-spin interactions of other reduced centres within the SerABC complex. In order to demonstrate the involvement of both [3Fe-4S] and [4Fe-4S] clusters in electron transfer during selenate turnover, the reduced sample was thawed under nitrogen and treated with selenate and subsequently rapidly (within 5 seconds) refrozen. The selenate re-oxidised spectrum recorded at 10K clearly shows selenate dependent re-oxidation of the $[4Fe\text{-}4S]^{1+}$ cluster rendering most of its signal EPR silent, with the concomitant re-oxidation of the [3Fe-4S] cluster re-generating the S=1/2 signal at g_{av}~2.01 (Figure 4). This suggests that both types of iron-sulfur clusters play a functional role in electron transfer to the selenate reductase active site and that the [3Fe-4S] cluster observed is not due to iron loss from a more typical [4Fe-4S] cluster. The SerABC samples were electrochemically poised at a range of potentials between ±400 mV. The $[3Fe\text{-}4S]^{1+}$ cluster EPR signal was lost between the potential range 400 to 0 mV, and the titration could be fitted with a simple *n* = 1 Nernstian curve from which a midpoint potential of +118 ± 10 mV for the $[3Fe\text{-}4S]^{0/1+}$ couple could be derived (Figure 5B). The $[4Fe\text{-}4S]^{1+}$ cluster EPR signal developed over a range of potentials between ±300 mV and was best fitted with two sequential Nernstian *n* = 1 curves with midpoint redox potentials of +183 ± 10 mV and -51 ± 10 mV for the two $[4Fe\text{-}4S]^{1+/2+}$ cluster couples. Double integration of this signal yielded a spin concentration representing a population of ~1.5 [4Fe-4S] clusters per SerABC unit. Upon further reduction to <-300 mV

the observed signal intensity of the $[4Fe\text{-}4S]^{1+}$ cluster decreases. This change in intensity can again be fitted to an *n*=1 Nernstian component with a mid-point potential of E_m~-356 ± 10 mV mV (Figure 5B).

The N-terminal domain of the membrane-bound nitrate reductase (NarG) displays a conserved cysteine rich motif ($HX_3CX_3CX_{35}C$) that is involved in the co-ordination of an iron-sulfur cluster (FS0) of the [4Fe-4S] type, yet attempts to detect the cluster in early EPR studies were unsuccessful [33,34]. The involvement of this motif in the co-ordination of a [4Fe-4S] cluster was only demonstrated in the recent crystal structures of NarG from *E. coli* [12,13]. A similar structural coordination for FS0 has now also been shown in *A. aromaticum* EbdA [20]. The FS0 cluster has novel co-ordination provided by the three cysteine ligands with an additional histidine ligand positioned at residue His^{49}. It was suggested that such co-ordination might give rise to unusual spectroscopic properties [12]. Subsequent EPR studies of NarG [35] have now shown that FS0 has an unusual high-spin (S=3/2) ground state, giving rise to an EPR signal in the g~5 region of the spectrum. By recording the EPR spectrum at low temperature (5K) and high power (100mW), signals at g~5.023 and g~5.556 were readily detected in dithionite reduced NarG [35]. A similar cluster in SerA is also presumed to be co-ordinated by one histidine and three cysteine ligands since the motif is conserved. Assuming that FS0 in SerA might also have an unusual high-spin ground state we have also investigated the selenate reductase complex under similar conditions. Whilst a broad feature is observed between 160-180 mT, no peaks at g~5 or 5.5 are observed typical of a high-spin cluster (data not shown). Whilst it was noted by Rothery *et al*. [35], that the FS0 was not observed in apomolybdo-NarGHI, low molybdenum occupancy (~50%) in SerA might also point to low occupancy of FS0, but the total metal content would suggest otherwise. Given that the metal analysis indicates Fe occupancy consistent with 5xFeS cluster and that the selenate-dependent re-oxidation of the redox centres of SerB are observed, it would suggest that FS0 is probably present, but in an undetectable state, possibly having a lower equilibrium potential than can be reached by reduction with sodium dithionite.

EPR studies of haem-b

The full-sweep EPR spectrum of the "as prepared" selenate reductase complex revealed a small positive peak at g~3.33. Closer inspection of the selenate re-oxidised sample (Fig 6) showed that this signal had increased in intensity and its line-shape is considered typical of the g_3 feature of a rhombic trio, possibly with the g_2 and g_1 resonances either hidden under those

Biochemical Journal Immediate Publication. Published on 10 Aug 2007 as manuscript BJ20070669

arising from the $[3Fe\text{-}4S]^{1+}$ cluster or are too broad to be observed at X-band. The g_3 signal is similar to a feature observed in the dimethyl sulfide dehydrogenase (DMSDH), that has been studied further by magnetic circular dichroism spectroscopy and been assigned to the g_3 feature of the spectrum of low-spin ferric haem-*b* in the γ-subunit [17]. It would thus seem appropriate that the same g_3 signal can be attributed to a low-spin ferric haem-*b* in SerC.

EPR studies of the molybdenum centre of SerA

The EPR spectrum of the as prepared SerABC complex recorded at 60K is dominated by resonances, with g-anisotropy consistent with a Mo(V) centre containing a single d^1 unpaired electron (S=1/2) (Figure 7) (Table 1). The spectrum has principal g values of g_3~1.999, g_2~1.996 and g_1~1.965 (g_{av} 1.9867). Comparison of the spectroscopic parameters with other molybdoenzymes shows that the anisotropy of the Mo(V) signal is similar to values reported for other members of the Type II group (Table 1). However, the rhombicity of the signal is notably lower than that from most other members of this group except for the value reported [36] for DmsA from *E. coli*. The sample was poised at pH 6.0 and the dominant features at g_2 and g_3 do not resolve splittings consistent with proton hyperfine coupling. Hyperfine splitting is observed in the g_1 region of the Mo(V) spectrum and can be best simulated as arising from a single proton nucleus (I = 1/2) with a coupling constant of A_1 (^{1}H) = 1.014 [mT]. A splitting of 1.014 mT is consistent with that caused by a proton of an equatorial hydroxyl ligand to the Mo(V) centre [37] and is in agreement with the postulated structure of the active site derived from EXAFS [8], that places a bound hydroxyl ligand with a short Mo-O bond of 1.81Å. A second, much less intense spectrum is also observed with resonances at higher field (A ~ 4mT) and probably arises from a mixture of natural molybdenum isotopes (^{95,97}Mo, I = 5/2). Upon reduction with dithionite (Figure 8) there is a decrease in the intensity of the g_3~1.999 signal and a loss of the feature at g_2 ~1.965. Treatment of the sample with selenate appears to again enhance features at g_3~1.999 and g_1~1.965, suggesting that the observed Mo(V) species is formed as an intermediate during selenate turnover. However, the selenate re-oxidised spectrum clearly shows a sharper feature at g ~2.008 and the g_1~1.965 feature is no longer split by a proton, and as such might represent a SeO_4^{2-} bound intermediate. Experiments to determine the redox potential for the Mo(IV)/Mo(V) and Mo(V)/Mo(VI) couples were not possible at this stage due to insufficient material to produce a series of electrochemically poised samples at concentrations required to observe a resolvable Mo(V) signal.

Biochemical Journal Immediate Publication. Published on 10 Aug 2007 as manuscript BJ20070669

Discussion

In the present work we have undertaken a detailed spectroscopic study of the redox cofactors of the periplasmic selenate reductase from *T. selenatis* and the results presented have resolved signals attributed to centres $[3Fe\text{-}4S]^{1+}$, $[4Fe\text{-}4S]^{1+}$, Mo(V) and haem-*b*. Selenate reductase is a member of an expanding group of molybdo-enzymes, which based upon sequence alignments have tentatively been assigned to the Type II clade. The Type II members are a distinct subgroup that include; nitrate reductase (nNAR and pNAR), ethylbenzene dehydrogenase (EBDH), dimethylsulfoxide reductase (DmsABC) and dimethyl sulfide dehydrogenase (DMSDH). This group all have a number of common features. Sequence analysis of the catalytic subunits, for example, shows that an aspartate residue is highly conserved amongst this group and in the recent crystal structures of nitrate reductase (NarGH and NarGHI) [12,13] and ethylbenzene dehydrogenase [20] it has been shown to co-ordinate directly to the Mo centre. This is in contrast to members of the Type I and Type III molybdo-enzymes. In the Type I enzymes, the Mo centre either has no ligand, as is the case for arsenite oxidase, or is liganded via a cysteine (e.g. NAP) or selenocysteine (e.g. FDH). In the Type III enzymes, the Mo centre is co-ordinated via a serine ligand (e.g. DMSO reductase). The distinction of the different co-ordination types observed in the structures of the active sites of these molybdo-enzymes is also evident in the EPR parameters recorded for their Mo(V) species [17]. Consequently, it was expected that the Mo(V) EPR signals for selenate reductase would be similar to those of other Type II molybdo-enzymes. The combined evidence from all the EPR parameters; g_{av}, anisotropy and rhombicity, show that selenate reductase is indeed better grouped as a Type II enzyme. In light of the recent crystal structures of NarGH (and NarGHI) from *E. coli* and EBDH from *A. aromaticum*, the present spectroscopic work provides strong evidence that selenate reductase is correctly grouped and is also likely to have the Mo centre co-ordinated directly by the highly conserved Asp positioned at residue 209 in the SerA sequence. However, it is noted that in the EXAFS analysis of selenate reductase by Maher *et al*., [8] no evidence was presented in support of an aspartate ligand to Mo and the authors speculated that the structure of the active site might resemble that of the Type I enzyme, arsenite oxidase, with a *bis*-MGD cofactor in which Mo is not ligated directly via an amino acid ligand [38]. Unfortunately, no comparisons can be made between the Mo(V) EPR spectra of selenate reductase and arsenite oxidase since the Mo(V) species in arsenite oxidase is inherently unstable [39]. Consequently, the one electron reduced Mo(V) state does not accumulate and no Mo(V) EPR spectrum has yet been detected [39]. The fact that selenate reductase loses the Mo cofactor during purification, suggests that any amino acid ligand

present might readily dissociate. The flexible co-ordination of the Asp ligand may be evident when considering the structures obtained for nitrate reductase; in the structure reported by Bertero *et al*. [12], the Mo is co-ordinated by six ligands, four *cis*-dithiolene sulfur atoms from the *bis*-MGD and a bidentate ligand from both side chain oxygen atoms from the carboxylate group of Asp^{222}. In contrast, the structure reported by Jormakka *et al*. [13] has the Mo again co-ordinated by four *cis*-dithiolene sulfur atoms, but only a single carboxylate oxygen from Asp^{222}.

The amino acid sequence of SerB shows four potential iron-sulfur cluster binding motifs (Figure 9A). It is also predicted that an iron-sulfur cluster is coordinated to the N-terminal region of SerA. EPR spectroscopy in this study has clearly resolved two distinct signals that can be attributed to clusters of the [3Fe-4S] and [4Fe-4S] type. The [3Fe-4S] cluster is resolved in the oxidised protein and its EPR signal is lost upon reduction and redox titration reveals a midpoint potential of E_m~+118mV. An axial signal typical of a [4Fe-4S] cluster is observed upon reduction from +400 to -200 mV and the signal intensity can be fitted to two sequential n=1 Nernstian components with mid-point redox potentials of E_m~+183 mV and E_m~-51 mV. Upon further reduction to -400 mV, the observed signal intensity of the [4Fe-4S] cluster decreases. This change in intensity can again be fitted to an n=1 Nernstian component with a mid-point potential of E_m~-356 mV. It would appear from the redox titration that in SerB the three [4Fe-4S] clusters have very similar overlapping spectral features with a strong feature ($g_{1,2}$) at g~1.882. Upon reduction, two of the [4Fe-4S] clusters are clearly resolved, one at high potential (E_m~+183 mV) and the other at considerably lower potential (E_m~-51 mV). The resolution of the third cluster is apparent only by the decrease in signal intensity. It is considered likely that at very low redox potential E_m<-300 mV, the remaining oxidised cluster is reduced (S=1/2) and strongly spin-couples to a neighbouring $[4Fe\text{-}4S]^{1+}$ cluster rendering both centres EPR silent (net spin S=0), thus decreasing the observed signal intensity at g~1.882. Can these EPR signals be assigned to any particular clusters? If we consider the recent crystal structure from EBDH [20], we see that the β-subunit has a structure that resembles an N-terminal ferredoxin, containing two FeS clusters (termed FS1 and FS2) followed by a tandem repeat duplication, containing the second pair of FeS clusters (termed FS3 and FS4). The main difference between the two domains is that cluster FS4 is a [3Fe-4S] type coordinated by only three Cys ligands. SerB shares high sequence identity (55%) to the EBDH β-subunit and modelling the SerB structure on the EBDH β-subunit provides convincing evidence that the conserved Cys-rich motifs co-ordinate similar clusters (Figure

9B). Hence, we consider it highly likely that the $[3Fe\text{-}4S]^{1+}$ EPR spectrum detected at g_{av}~2.01 arises from the oxidised cluster FS4 coordinated residues at positions Cys^{145}, Cys^{166} and Cys^{172} (Figure 9C). The other [4Fe-4S] clusters form a sequential numbered (FS3-FS2-FS1) electron conduit through the protein transferring electrons to FS0 and MGD in SerA. SerB and EBDH β-subunit also show homology to the NarH component of the respiratory nitrate reductase, which has been the subject of extensive spectroscopic analysis. The mid-point potentials for the clusters in NarH have been resolved and have E_m values of +130 mV (FS1), -420 mV (FS2), -55 mV (FS3) and +180 mV (FS4 - the [3Fe-4S] cluster) [40]. Therefore by analogy we suggest that in SerB the cluster potentials are +183 mV (FS1), -356 mV (FS2), -51 mV (FS3) and +118 mV (FS4) (Figure 10). So which centres are spin coupled in the fully reduced sample? It is noted in the crystal structure of EBDH that all the FeS clusters (FS1, FS2, FS3 and FS4) are in close contact (<6.9Å apart). However, the structure shows that clusters FS2 and FS3 (5.4Å apart) are closer together by 1.1Å than clusters FS1 and FS2 (6.6Å apart). It would thus seem most likely that in the fully reduced sample, FS2 and FS3 would be spin coupled. Consequently, we assign the detectable [4Fe-4S] cluster (with EPR features at $g_{1,2}$~1.882 and g_3~2.026) in the fully reduced sample to cluster FS1 and speculate that in SerB it is co-ordinated by residues at positions Cys^{15}, Cys^{18}, Cys^{21} and Cys^{212} (Figure 9C).

The EPR signal seen at g~3.33 in the as prepared sample increased in intensity upon selenate re-oxidation. This signal is very similar to a feature observed in DMSDH, that based upon subsequent MCD analysis, has been assigned to the g_3 feature of the spectrum of low-spin ferric haem-*b* with histidine and methione axial ligands [17]. We therefore suggest that the g~3.33 signal seen in selenate reductase also arises due to the presence of the haem-*b* in SerC, but given the close sequence similarity amongst a number of Tat-translocated D-group molybdoenzymes [11], it is consider more likely that the Fe^{III} is coordinated by the highly conserved methionine (Met^{137}) and lysine (Lys^{228}) residues, as recently demonstrated in the structure of the γ subunit of EBDH [20]. Upon purification, the SerC haem is partially reduced whilst other detectable redox centres appear oxidised, indicating that the *b*-haem in SerC might have a relatively high redox potential. Complete oxidation is achieved by the addition of selenate, demonstrating its involvement of electron transfer to SerAB (not shown). The similar haem moiety in DMSDH also has a high-redox potential (+315 mV) [17] and these studies have suggested that this will help facilitate its role in electron transfer out of the enzyme to a periplasmic electron acceptor. Clearly, selenate reductase works in the reverse direction, transferring electrons via the redox centres to the active site of SerA. The means by which

selenate reductase obtains its electrons is currently unknown, but a *c*-type cytochrome (23 kDa) co-purifies with the reductase complex following ammonium sulphate precipitation and hydrophobic interaction chromatography and has been demonstrated to act as an electron donor to the reductase *in vitro* (Lowe EC, Bydder S, Santini JM, Butler CS, unpublished results). It is presumed that electrons enter the selenate reductase via SerC and the presence of a high-potential *b*-haem might facilitate electron transfer from a number of different redox partners.

In summary, this work provides the first spectro-potentiometric insight into an enzyme that catalyses a key reductive reaction in the biogeochemical selenium cycle. The variable temperature EPR spectra of the purified selenate reductase complex has revealed features attributable to centres $[3Fe\text{-}4S]^{1+}$, $[4Fe\text{-}4S]^{1+}$, Mo(V) and haem-*b*. The involvement of the [3Fe-4S] and [4Fe-4S] clusters in electron transfer to the active site of selenate reductase was demonstrated by the re-oxidation of both clusters under selenate turnover conditions. The combined evidence from EPR spectroscopy and redox potentiometry has revealed four of the five FeS clusters in SerABC, with only FS0 in SerA remaining undetected. The Mo(V) EPR recorded at 60K, gives rise to spectral features similar to those obtained for other aspartate liganded (D-group) molybdoenzymes and provides good evidence in support of the assignment of the periplasmic selenate reductase as a member of the Type II molybdo-enzymes.

Acknowledgments

This work was funded in part by research grants from the BBSRC (P13842, P17219 and BBS/B/10110) to CSB and DJR. EJD was a recipient of a BBSRC PMS committee studentship. We thank Ann Reilly (University of East Anglia) and Helen Ridley (University of Newcastle) for technical assistance. We are grateful to Dr Megan Maher (Imperial College, University of London), Prof. Alastair McEwan and Dr Paul Bernardt (University of Queensland) for helpful discussions.

References

1. Stolz, J.F. and Oremland, R.S. (1999) Bacterial respiration of arsenic and selenium. FEMS Microbiol. Rev. **23,** 615-627
2. Stolz, J.F., Basu, P., Santini, J.M. and Oremland, R.S. (2006) Arsenic and selenium in microbial metabolism. Annu. Rev. Microbiol. **60**, 107-30

3. Heider, J. and Bock, A. (1993) Selenium metabolism in micro-organisms. Adv. Microb. Physiol. **35**, 71-109
4. Schröder, I., Rech, S., Krafft, T. and Macy, J.M. (1997) Purification and characterization of the selenate reductase from *Thauera selenatis*. J. Biol. Chem. **272,** 23765-23768
5. Ridley, H., Watts, C.A., Richardson, D.J. and Butler, C.S. (2006) Resolution of distinct membrane-bound enzymes from *Enterobacter cloacae* SLD1a-1 responsible for the selective reduction of nitrate and selenate. Appl. Environ. Micro. **72**, 5173-5180
6. Macy, J.M., Rech, S., Auling, G., Dorsch, M., Stackenbrandt, E. and Sly, L.I. (1993) *Thauera selenatis* gen-nov, sp-nov, a member of the beta-subclass of proteobacteria with a novel type of anaerobic respiration. Int. J. Syst. Bacteriol. **43,**135-142
7. Krafft, T., Bowen, A., Theis, F. and Macy, J.M. (2000) Cloning and sequencing of the genes encoding the periplasmic-cytochrome B-containing selenate reductase of *Thauera selenatis*. DNA Seq. **10**,365-377
8. Maher, M.J., Santini, J., Pickering, I.J., Prince, R.C., Macy, J.M. and George, G.N. (2004) X-ray absorption spectroscopy of selenate reductase. Inorg. Chem. **43,** 402-404
9. Trieber, C.A., Rothery, R.A. and Weiner, J.H. (1996) Engineering a novel iron-sulfur cluster into the catalytic subunit of *Escherichia coli* dimethyl-sulfoxide reductase. J. Biol. Chem. **271**, 4620-4626
10. McDevitt, C.A., Hugenholtz, P., Hanson, G.R. and McEwan, A.G. (2002) Molecular analysis of dimethyl sulphide dehydrogenase from *Rhodovulum sulfidophilum*: its place in the dimethyl sulphoxide reductase family of microbial molybdopterin-containing enzymes. Mol. Microbiol. **44**, 1575-1587
11. Martinez-Espinosa, R.M., Dridge, E.J., Bonete, M.J., Butt, J.N., Butler, C.S., Sargent, F. and Richardson, D.J. (2007) Look on the positive side! The orientation, identification and bioenergetics of "Archaeal" membrane-bound nitrate reductases. FEMS Microbiol. Lett. (minireview) *in press*
12. Bertero, M.G., Rothery, R.A., Palak, M., Hou, C., Lim, D., Blasco, F., Weiner, J.H. and Strynadka, N.C. (2003) Insights into the respiratory electron transfer pathway from the structure of nitrate reductase A. Nat. Struct. Biol. **10**, 681-687
13. Jormakka, M., Richardson, D.J., Byrne, B. and Iwata, S. (2004) The Architecture of NarGH reveals a structural classification of MGD enzymes. Structure **12**, 95-104
14. Sargent, F. (2007) Constructing the wonders of the bacterial world: biosynthesis of complex enzymes. Microbiology SGM **153**,633-651

15. Berks, B.C., Sargent, F. and Palmer, T. (2000) The Tat protein export pathway. Mol Microbiol **35**, 260-274.
16. Thorell, H.D., Stenklo, K., Karlsson, J. and Nilsson, T. (2003) A gene cluster for chlorate metabolism in *Ideonella dechloratans*. Appl. Environ. Microbiol. **69**, 5585-5592
17. McDevitt, C.A., Hanson, G.R., Noble, C.J., Cheesman, M.R. and McEwan, A.G. (2002) Characterization of the redox centers in dimethyl sulfide dehydrogenase from *Rhodovulum sulfidophilum*. Biochemistry **41**, 15234-15244
18. Bender, K.S., Shang, C., Chakraborty, R., Belchik, S.M., Coates, J.D. and Achenbach, L.A. (2005) Identification, characterization, and classification of genes encoding perchlorate reductase. J. Bacteriol. **187**, 5090-5096
19. Johnson, H.A., Pelletier, D.A. and Spormann, A.M. (2001) Isolation and characterization of anaerobic ethylbenzene dehydrogenase, a novel Mo-Fe-S enzyme. J. Bacteriol. **183,** 4536-4542
20. Kloer, D.P., Hagel, C., Heider, J. and Schulz, G.E. (2006) Crystal structure of ethylbenzene dehydrogenase from *Aromatoleum aromaticum.* Structure **14**, 1377-1388
21. Richardson, D.J., Berks, B.C., Spiro, S., Russell, D.A. and Taylor, C.J. (2001) The Biochemical, genetic and physiological diversity of prokaryotic nitrate reduction. Cellular and Molecular Life Sciences **58**, 165-178
22. Dridge, E.J., Richardson, D.J., Lewis, R.J. and Butler, C.S. (2006) Developing structure-based models to predict substrate specificity of D-group (Type II) molybdenum enzymes: application to a molybdo-enzyme of unknown function from *Archaeoglobus fulgidus*. Biochem. Soc. Trans. **34**, 118-121
23. Ridley, H., Watts, C.A., Richardson, D.J. and Butler, C.S. (2006) Development of a viologen based microtitre plate assay for the analysis of oxyanion reductase activity: Application to the membrane bound selenate reductase from *Enterobacter cloacae* SLD1a-1. Anal. Biochem. **358**, 289-294
24. Bennett, B., Berks, B.C., Ferguson, S.J., Thomson, A.J. and Richardson, D.J. (1994) Mo(V) electron paramagnetic resonance signal from the periplasmic nitrate reductase of *Thiosphaera pantotropha*. Eur. J. Biochem. **226**, 789-798
25. Butler, C.S., Charnock, J.M., Bennett, B., Sears, H.J., Reilly, A.J., Ferguson, S.J., Garner, C.D., Lowe, D.J., Thomson, A.J., Berks, B.C. and Richardson, D.J. (1999) Models for molybdenum co-ordination during the catalytic cycle of periplasmic nitrate reductase from *Paracoccus denitrificans* derived from EPR and EXAFS spectroscopy. Biochemistry **38,** 9000-9012

26. Jepson, B., Anderson, L., Rubio, L.M., Taylor, C.J., Butler, C.S., Flores, E., Herrero, A., Butt, J. and Richardson, D.J. (2004) Tuning a nitrate reductase for function: the first spectro-potentiometric characterisation of a bacterial assimilatory nitrate reductase reveals novel redox properties. J. Biol. Chem. **279**, 32212-32218
27. Morris, A.L., MacArthur, M.W., Hutchinson, E.G. and Thornton, J.M. (1992). Stereochemical quality of protein structure coordinates. Proteins **12**, 345-364
28. Laskowski, R.A., MacArthur, M.W., Moss, D.S. and Thornton, J.M. (1993). PROCHECK: a program to check the stereochemical quality of protein structures. J. Appl. Cryst. **26**, 283-291
29. DeLano, W.L. (2002) The PyMOL Molecular Graphics System, DeLano Scientific, San Carlos, CA, USA. http://www.pymol.org
30. Caradoc-Davies, T.T., Cutfirld, S.M., Lamont, I.L. and Cutfield, J.F. (2004) Crystal structures of *Escherichia coli* uridine phosphorylase in two native and three complexed forms reveal basis of substrate specificity, induced conformational changes and influence of potassium. J. Mol. Biol. **337**, 337-354
31. Cammack, R. (1992) Iron-sulphur clusters in enzymes - themes and variations. Adv. Inorg. Chem. **38**, 281-322
32. Mouesca, J.M., Noodleman, L., Case, D.A. and Lamotte, B. (1995) Spin densities and spin coupling in iron–sulfur cluster: a new analysis of hyperfine coupling constants. Inorg. Chem. **34**, 4347-4359
33. Magalon, A., Asso, M., Guigliarelli, B., Rothery, R.A., Bertrand, P., Giordano, G. and Blasco, F. (1998) Molybdenum cofactor properties and [Fe-S] cluster coordination in *Escherichia coli* nitrate reductase A: investigation by site-directed mutagenesis of the conserved His-50 residue in the NarG subunit. Biochemistry **37**, 7363-7370
34. Guigliarelli, B., Magalon, A., Asso, M., Bertrand, P., Frixon, C., Giordano, G. and Blasco, F. (1996) Complete coordination of the four Fe-S centres of the β-subunit from *Escherichia coli* nitrate reductase. Physiological, biochemical and EPR characterisation of site-directed mutants lacking the highest or lowest potential [4Fe-4S] clusters. Biochemistry **35**, 4828-4836
35. Rothery, R.A., Bertero, M.G., Cammack, R., Palak, M., Blasco, F., Strynadka, N.C.J. and Weiner, J.H. (2004) The catalytic subunit of *Escherichia coli* nitrate reductase A contains a novel [4Fe-4S] cluster with a high-spin ground state. Biochemistry **43**, 5324-5333

36. Rothery, R.A., Trieber, C.A. and Weiner, J.H. (1999) Interactions between the molybdenum cofactor and iron-sulfur clusters of *Escherichia coli* dimethylsulfoxide reductase. J. Biol. Chem. **274**, 13002-13009

37. Bray, R.C. (1988) The inorganic biochemistry of molybdoenzymes. Q. Rev. Biophys. **21**, 299-329

38. Conrads, T., Hemann, C., George, G.N., Pickering, I.J., Prince, R.C. and Hille R. (2002) The active site of arsenite oxidase from *Alcaligenes faecalis*. J. Am. Chem. Soc. **124**, 11276-11277

39. Hoke, K.R., Cobb, N., Armstrong, F.A. and Hille, R. (2004) Electrochemical studies of arsenite oxidase: an unusual example of a highly cooperative two-electron molybdenum center. Biochemistry **43**, 1667-1674

40. Rothery, R.A., Magalon, A., Giordano, G., Guigliarelli, B., Blasco, F. and Weiner, J.H. (1998) The molybdenum cofactor of *Escherichia coli* nitrate reductase A (NarGHI). Effect of a mobAB mutation and interactions with [Fe-S] clusters. J. Biol. Chem. **273**, 7462-7469

41. Guigliarelli, B., Asso, M., More, C., Augher, V., Blasco, F., Pommier, J., Giordano, G. and Bertrand, P. (1992) EPR and redox characterization of iron-sulfur centers in nitrate reductases A and Z from *Escherichia coli*. Evidence for a high-potential and a low-potential class and their relevance in the electron-transfer mechanism. Eur. J. Biochem. **207**, 61-68

42. Yoshimatsu, K., Iwasaki, T. and Fujiwara T. (2002) Sequence and electron paramagnetic resonance analyses of nitrate reductase NarGH from a denitrifying halophilic euryarchaeote *Haloarcula marismortui*. FEBS lett. **516**, 145-150

43. Cammack, R. and Weiner, J.H. (1990) Electron paramagnetic resonance spectroscopic characterization of dimethyl sulfoxide reductase of *Escherichia coli*. Biochemistry **29**, 8410-8416.

44. Costa, C., Teixeira, M., LeGall, J., Moura, J.J.G. and Moura, I. (1997) Formate dehydrogenase from *Desulfovibrio desulfuricans* ATCC 27774: Isolation and spectroscopic characterization of the active sites (heme, iron-sulfur centers and molybdenum). J. Biol. Inorg. Chem. **2**, 198-208

45. George, G.N., Bray, R.C., Morpeth, F.F. and Boxer, D.H. (1985) Complexes with halide and other anions of the molybdenum centre of nitrate reductase from *Escherichia coli.* Biochem. J. **227**, 925-931

46. George, G.N., Turner, N.A., Bray, R.C., Morpeth, F.F., Boxer, D.H. and Cramer, S.P. (1989) X-ray-absorption and electron-paramagnetic-resonance spectroscopic studies of the environment of molybdenum in high-pH and low-pH forms of *Escherichia coli* nitrate reductase. Biochem. J. **259**, 693-700

47. Bennett, B., Benson, N., McEwan, A.G. and Bray, R.C. (1994) Multiple states of the molybdenum centre of dimethylsulphoxide reductase from *Rhodobacter capsulatus* revealed by EPR spectroscopy. Eur. J. Biochem. **225**, 321-331

48. McEwan, A.G., Pride, J.P., McDevitt, C.A. and Hugenholtz, P. (2002) The DMSO reductase family of microbial molybdenum enzymes; molecular properties and role in the dissimilatory reduction of toxic elements. Geomicrobiology Journal, **19**, 3-21

49. Cheng, V.W.T., Rothery, R.A., Bertero, M.G., Strynadka, N.C.J. and Weiner, J.H. (2005) Investigation of the environment surrounding iron-sulfur cluster 4 of Escherichia coli dimethylsulfoxide reductase. Biochemistry **44**, 8068-8077

Biochemical Journal Immediate Publication. Published on 10 Aug 2007 as manuscript BJ20070669

Table 1. Spectroscopic parameters for the redox centres of selenate reductase and their comparison to other related molybdo-enzymes

Enzyme Class	Membrane orientation	Enzyme/ sample	Redox centre	g_1	g_2	g_3	g_{av}	Δg for [4Fe-4S]	Anisotropy	Rhombicity	Reference
II	+	SerABC	$[3Fe\text{-}4S]^{1+}$	1.9910	2.0046	2.0260	2.0072	-	0.035	0.611	This work
II	+	DMSDH[1]	$[3Fe\text{-}4S]^{1+}$	1.9650	1.9870	2.0180	1.9900	-	0.053	0.585	[17]
II	+	SerABC	$[4Fe\text{-}4S]^{1+}$	1.8820	1.8820	2.0260	1.930	0.072	0.144	1.000	This work
II	+	DMSDH[1]	$[4Fe\text{-}4S]^{1+}$	1.8620	1.8870	2.0158	1.9216	0.081	0.154	0.837	[17]
II	+	NarGH[2†]	$[4Fe\text{-}4S]^{1+}$	1.88	1.95	2.05	1.960	0.042	0.17	0.647	[35,41]
II	-	NarGH[2‡]	$[4Fe\text{-}4S]^{1+}$	1.88	1.88	2.01	1.923	0.079	0.13	1.000	[35,41]
II	-	NarGH[3]	$[4Fe\text{-}4S]^{1+}$	1.8710	1.8850	2.0100	1.9220	0.080	0.139	0.899	[42]
III	+	DMSOR[4]	$[4Fe\text{-}4S]^{1+}$	1.8660	1.9300	2.0100	1.9353	0.067	0.144	0.556	[43]
I	+	FDH[5]	$[4Fe\text{-}4S]^{1+}$	1.8650	1.9260	2.0710	1.9500	0.052	0.206	0.643	[44]
I	+	NAP[6]	$[4Fe\text{-}4S]^{1+}$	1.8900	1.9400	2.030	1.9500	0.052	0.14	0.643	[24]
II	+	SerABC	Mo(V)	1.9650	1.9960	1.9990	1.9867	-	0.0340	0.09	This work
II	+	DMSDH[1]	Mo(V)-H_2O	1.9650	1.9846	2.0006	1.9834	-	0.0356	0.45	[17]
II	+	DMSDH[1]	Mo(V)-X	1.9600	1.9805	1.9989	1.9798	-	0.0389	0.47	[17]
II	+	DMSDH[1]	Mo(V)-OH	1.9627	1.980	1.9914	1.9785	-	0.0287	0.40	[17]
II	-	NarGH[2]	Mo(V) low pH	1.9642	1.9851	1.9997	1.9830	-	0.0355	0.41	[45,46]
II	-	DmsABC[7]	Mo(V)	1.960	1.980	1.984	1.9746	-	0.0240	0.167	[36]
III	+	DMSOR[4]	Mo(V) unsplit	1.9611	1.9833	1.9906	1.9783	-	0.0238	0.16	[47]
I	+	FDH[5]	Mo(V)	1.9630	1.9880	2.0190	1.9900	-	0.0560	0.55	[44]
I	+	NAP[6]	Mo(V)	1.9806	1.9902	1.9985	1.9898	-	0.0180	0.46	[25]

Table 1. Footnote:

Δg (g_e - g_{av}), Anisotropy ($g_3 - g_1$) and Rhombicity [(g_3 - g_2)/(g_3 - g_1)] parameters are provided to allow comparisons to be made between signals.

Membrane orientation (+/-) distinguishes proteins that are exported to the membrane potential positive side ($\Delta\psi$+) via the Tat-translocase.

Samples are as follows; [1]DMSDH, dimethyl sulfide dehydrogenase from *Rhodovulum. sulfidophilum*; [2]NarGH, membrane bound nitrate reductase from *E. coli*; [3]NarGH nitrate reductase from *Haloarcula marismortui*; [4]DMSOR, dimethylsulfoxide reductase from *Rhodobacter capsulatus*; [5]FDH, formate dehydrogenase from *Desulfovibrio desulfuricans*; [6]NAP, periplasmic nitrate reductase from *Paracoccus pantotrophus*; [7]DmsABC, dimethylsulfoxide reductase from *E. coli*.

Two different [4Fe-4S] signals have been observed for *E. coli* NAR and are represented as the †major conformation and ‡minor conformation [35,41].

Biochemical Journal Immediate Publication. Published on 10 Aug 2007 as manuscript BJ20070669

Figure legends

Figure 1. X-band EPR spectrum of the SER complex as prepared. Enzyme concentration was 70.4 μM in 50 mM PIPES (pH6.0). Conditions of measurement: microwave frequency, 9.38 GHz; microwave power, 2 mW; modulation amplitude, 0.5 mT; temperature 10K. 1 Scan. Inset shows SDS-PAGE resolved SER subunits (20μg total protein) stained with coomassie blue stain.

Figure 2. Temperature dependence of the $[3Fe\text{-}4S]^{1+}$ EPR spectrum. Enzyme concentration was 70.4 μM in 50 mM PIPES (pH6.0). Spectra recorded at the following temperatures; 10K (solid line); 12.5K (dashed line); 15K (dotted line); 20K (dash-dot line) and 25K (dash-dot-dot line). Conditions of measurement: microwave frequency, 9.38 GHz; microwave power, 2 mW; modulation amplitude, 0.5 mT. 1 Scan each. Offset spectrum shows the simulation of the experimental spectrum recorded at 10K.

Figure 3. Temperature dependence of the $[4Fe\text{-}4S]^{1+}$ EPR spectrum. Enzyme concentration was 70.4 μM in 50 mM PIPES (pH6.0). Samples were reduced by the addition of 10 mM sodium dithionite. Spectra recorded at the following temperatures; 10K (solid line); 20K (dashed line); 30K (dotted line) and 40K (dash-dot line). Conditions of measurement: microwave frequency, 9.38 GHz; microwave power, 2 mW; modulation amplitude, 0.5 mT. 1 Scan each. Offset spectrum shows the simulation of the experimental spectrum recorded at 10K.

Figure 4. Selenate-dependent re-oxidation of the [3Fe-4S] and [4Fe-4S] clusters. Enzyme concentration was 70.4 μM in 50 mM PIPES (pH6.0) prior to the addition of reactants. Both sodium dithionite and selenate where added to a final concentration of 10 mM. Dithionite reduced (solid line). Selenate re-oxidised under anoxic conditions (dash-dot-dot line). Conditions of measurement: microwave frequency, 9.38 GHz; microwave power, 2 mW; modulation amplitude, 0.5 mT; temperature 10K. 1 Scan each.

Figure 5. EPR monitored redox-potentitometric titration of the [3Fe-4S] and [4Fe-4S] clusters. (A) EPR spectra recorded from samples poised at different redox potentials from +400 to -400 mV. Enzyme concentration was ~10 μM in 50 mM PIPES (pH6.0) prior to the addition of reductant. (B) Change in signal intensity as a function of redox potential.

Normalised signal intensities (%) were determined by the change in intensity at the spectral positions indicated by the g values in (A) relative to the maximum intensity (100%) measured. The solid line in each case shows the best fit with n = 1 Nernstian components. Open triangles represent change in intensity at g~1.991 and closed triangles represent change in intensity at g~1.882.

Figure 6. EPR spectrum from selenate-oxidised SER complex revealing low-spin Fe(III) haem-*b*. Enzyme concentration was 70.4 μM in 50 mM PIPES (pH6.0). Conditions of measurement: microwave frequency, 9.38 GHz; microwave power, 2 mW; modulation amplitude, 1 mT; temperature 10K.

Figure 7. Mo(V) EPR spectrum from SER complex as prepared. Enzyme concentration was 70.4 μM in 50 mM PIPES (pH6.0). Conditions of measurement: microwave frequency, 9.38 GHz; microwave power, 2 mW; modulation amplitude, 0.5 mT; temperature 60K. 20 Scans. Spectra (a) experimentally recorded; (b) simulation of unsplit spectrum; (c) simulation with the presence of a single proton (I = 1/2) A_1 (^{1}H) = 1.014 [mT].

Figure 8. Mo(V) EPR spectra from SER complex under turnover conditions. Enzyme concentration was 70.4 μM in 50 mM PIPES (pH6.0). (a) As prepared oxidised; (b) dithionite reduced and (c) selenate re-oxidised. Conditions of measurement: microwave frequency, 9.38 GHz; microwave power, 2 mW; modulation amplitude, 0.5 mT; temperature 60K. 20 Scans each.

Figure 9. Co-ordination of FeS clusters in SerB. (A) SerB sequence showing cysteine rich motifs (underlined); (B) Predicted structure of SerB (right) modelled upon the crystal structure of EBDH β-subunit (left) [20]; (C) Putative SerB FeS cluster ligands.

Figure 10. Electron transfer through SerB (△), DmsB (■) and NarH (●). The E_m values of each of the [FeS] clusters is shown. Potentials displayed as substrate represent the mid-point potentials for the couples; selenate→selenite (Eo'~+475 mV), DMSO→DMS (Eo'~+160 mV) and nitrate→nitrite (Eo'~+430 mV). Q-pool indicates ubiquinol (Eo'~+65 mV) and menaquinol (Eo'~-55 mV) [48]. Arrows indicate direction of electron transfer. Data

for DmsB and NarH taken from reference [49]. The symbols α, β and γ indicate the interface between the three subunits of the enzyme complex.

Biochemical Journal Immediate Publication. Published on 10 Aug 2007 as manuscript BJ20070669

Figure 1. Dridge *et al*.

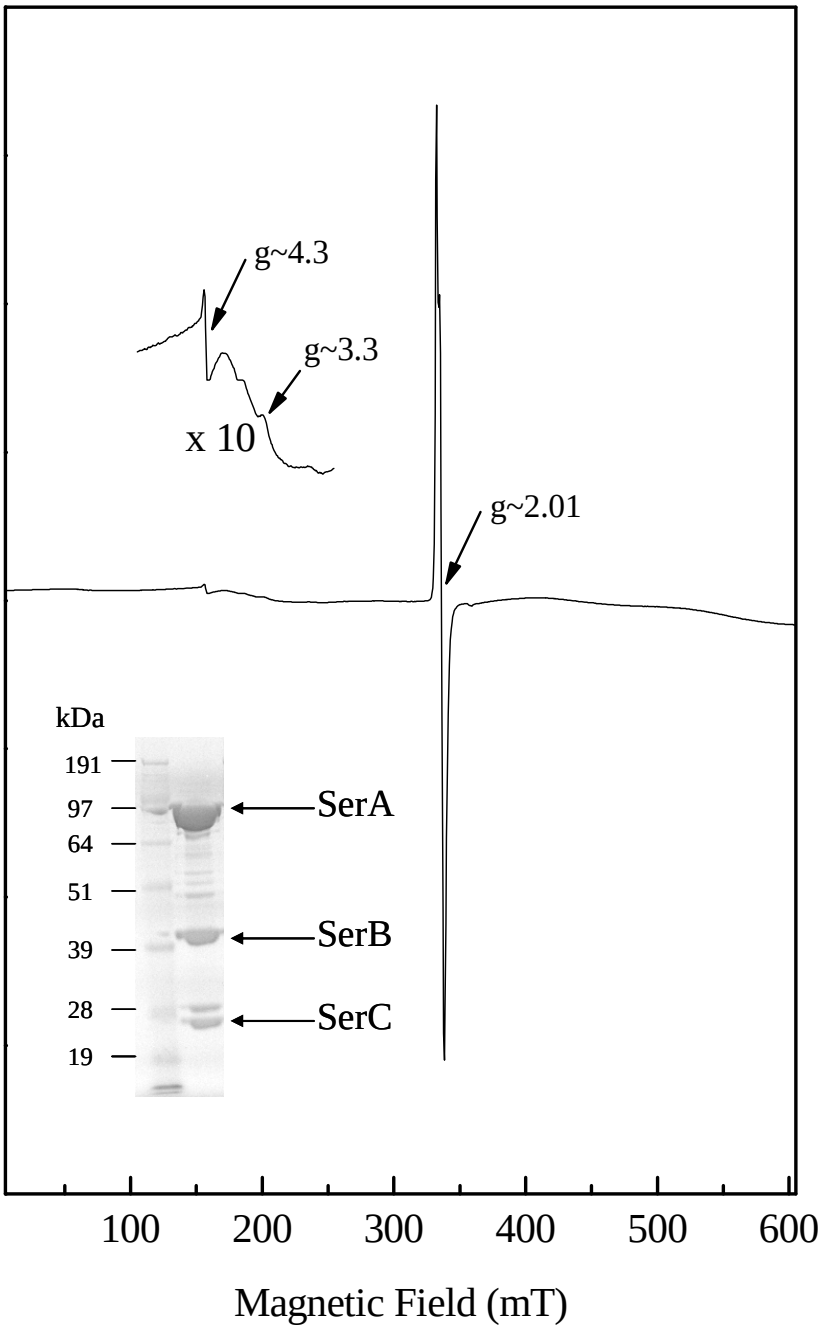

Biochemical Journal Immediate Publication. Published on 10 Aug 2007 as manuscript BJ20070669

Figure 2. Dridge *et al*.

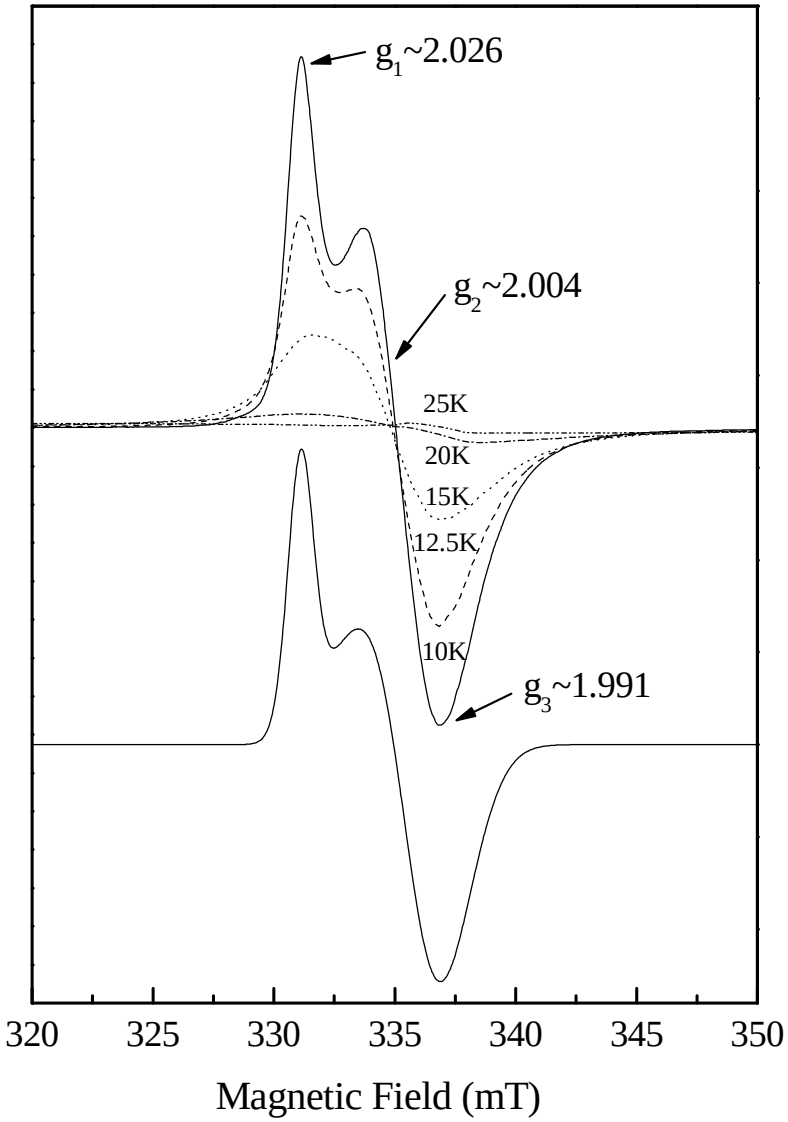

Biochemical Journal Immediate Publication. Published on 10 Aug 2007 as manuscript BJ20070669

Figure 3. Dridge *et al*.

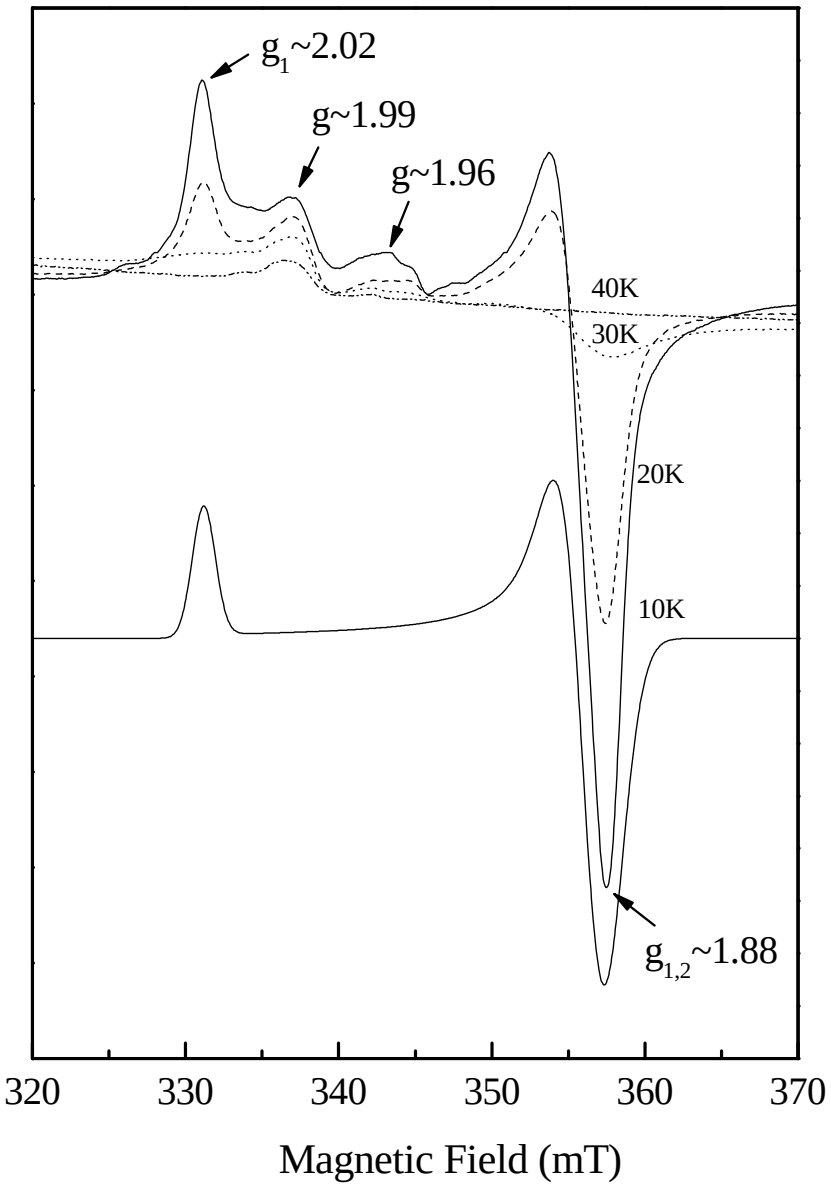

Biochemical Journal Immediate Publication. Published on 10 Aug 2007 as manuscript BJ20070669

Figure 4. Dridge *et al*.

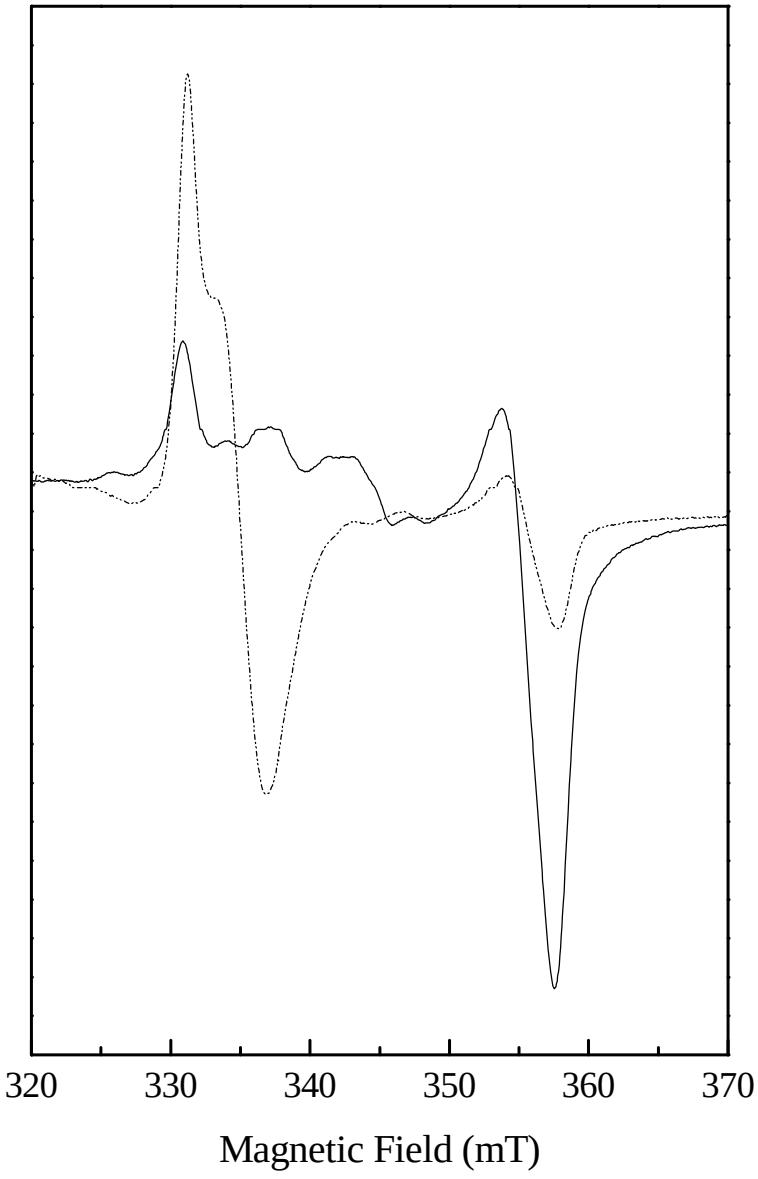

Biochemical Journal Immediate Publication. Published on 10 Aug 2007 as manuscript BJ20070669

Figure 5. Dridge *et al.*

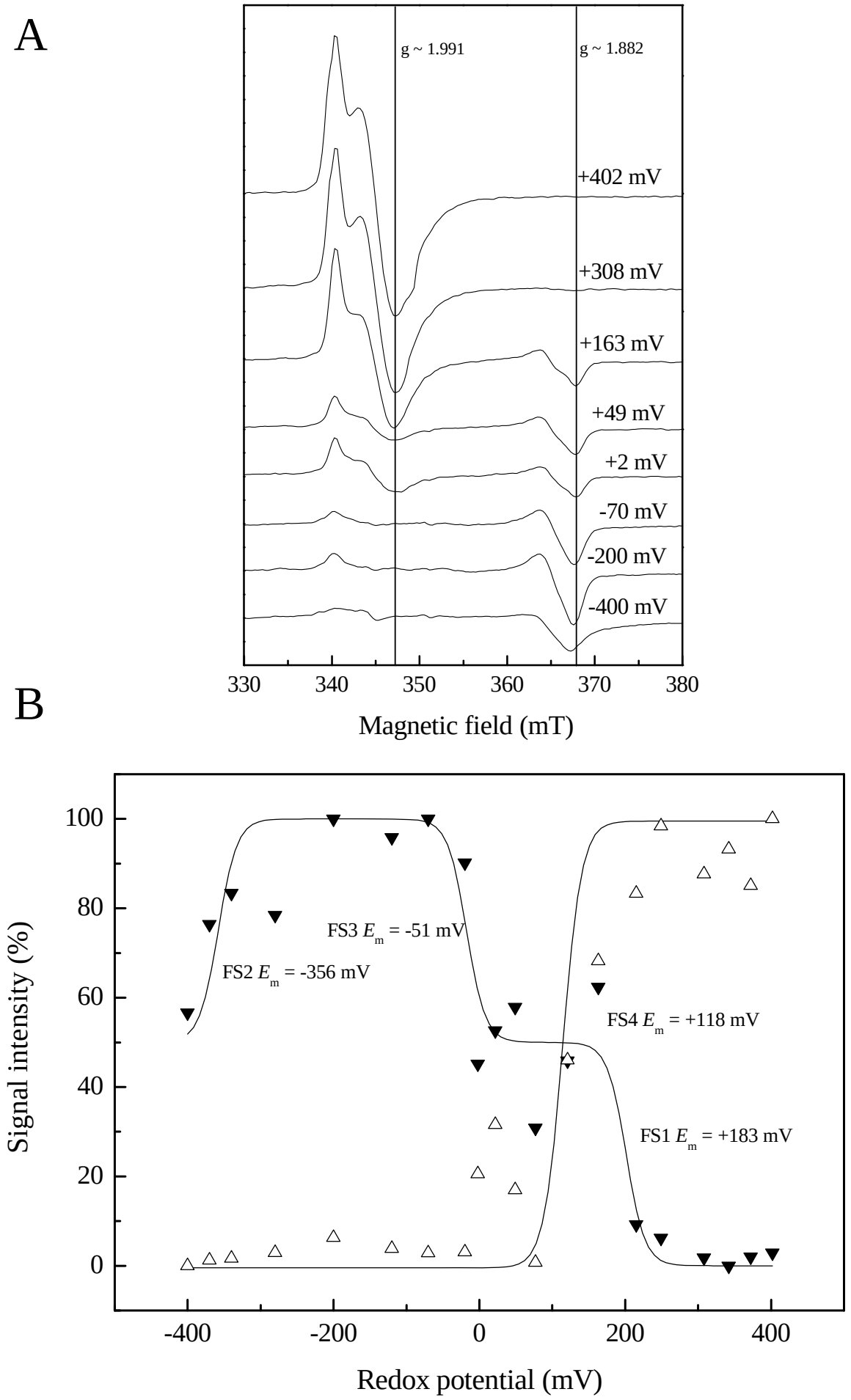

Biochemical Journal Immediate Publication. Published on 10 Aug 2007 as manuscript BJ20070669

Figure 6. Dridge *et al*.

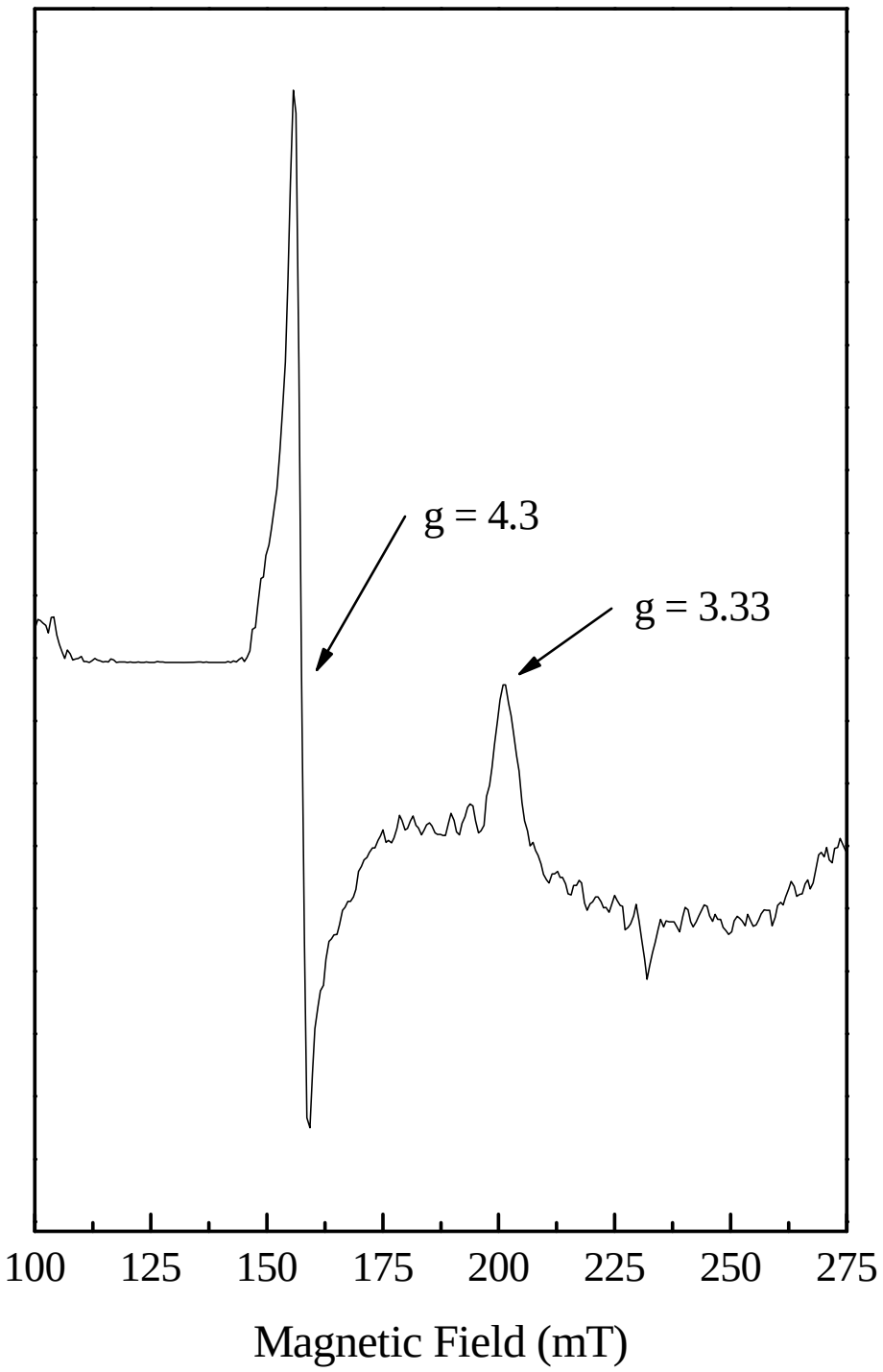

Biochemical Journal Immediate Publication. Published on 10 Aug 2007 as manuscript BJ20070669

Figure 7. Dridge *et al*.

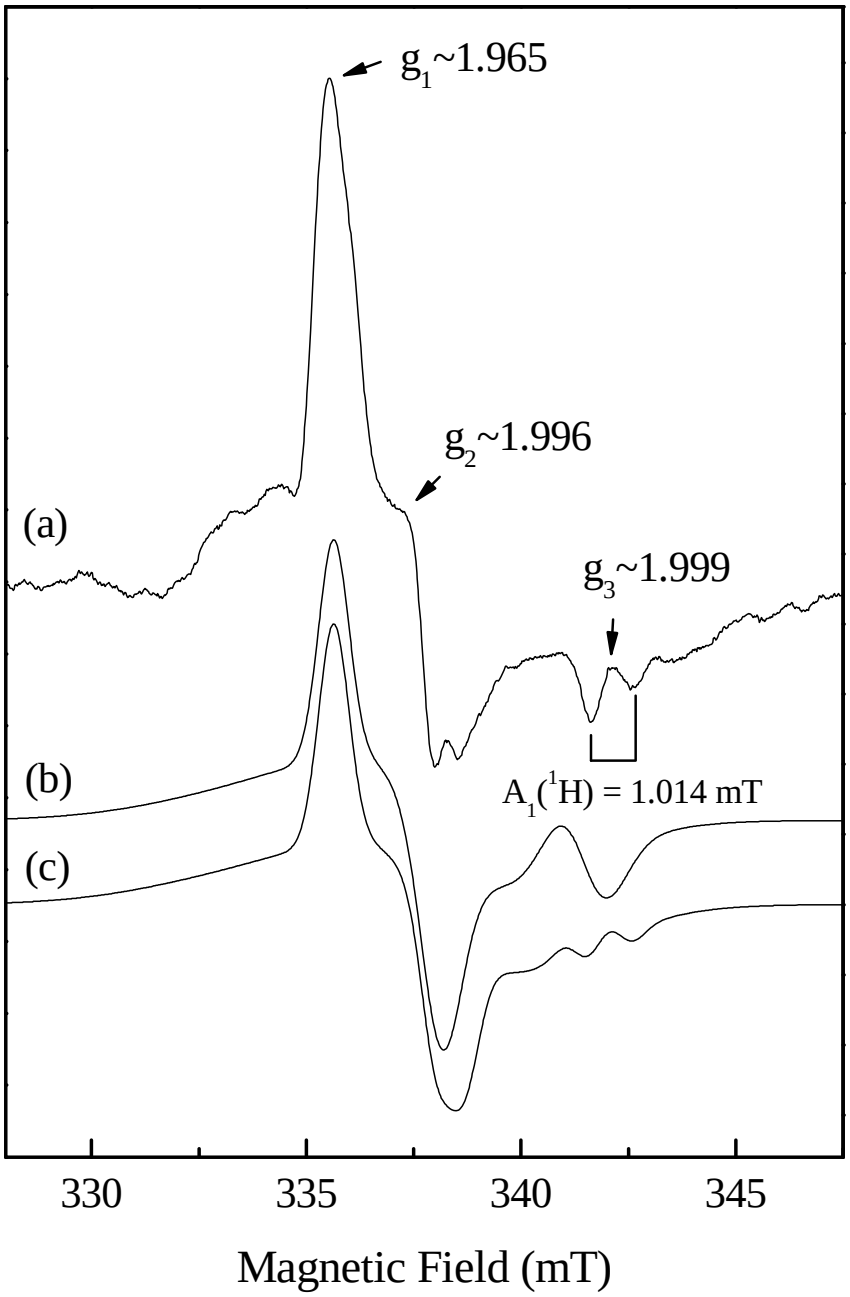

Biochemical Journal Immediate Publication. Published on 10 Aug 2007 as manuscript BJ20070669

Figure 8. Dridge *et al*.

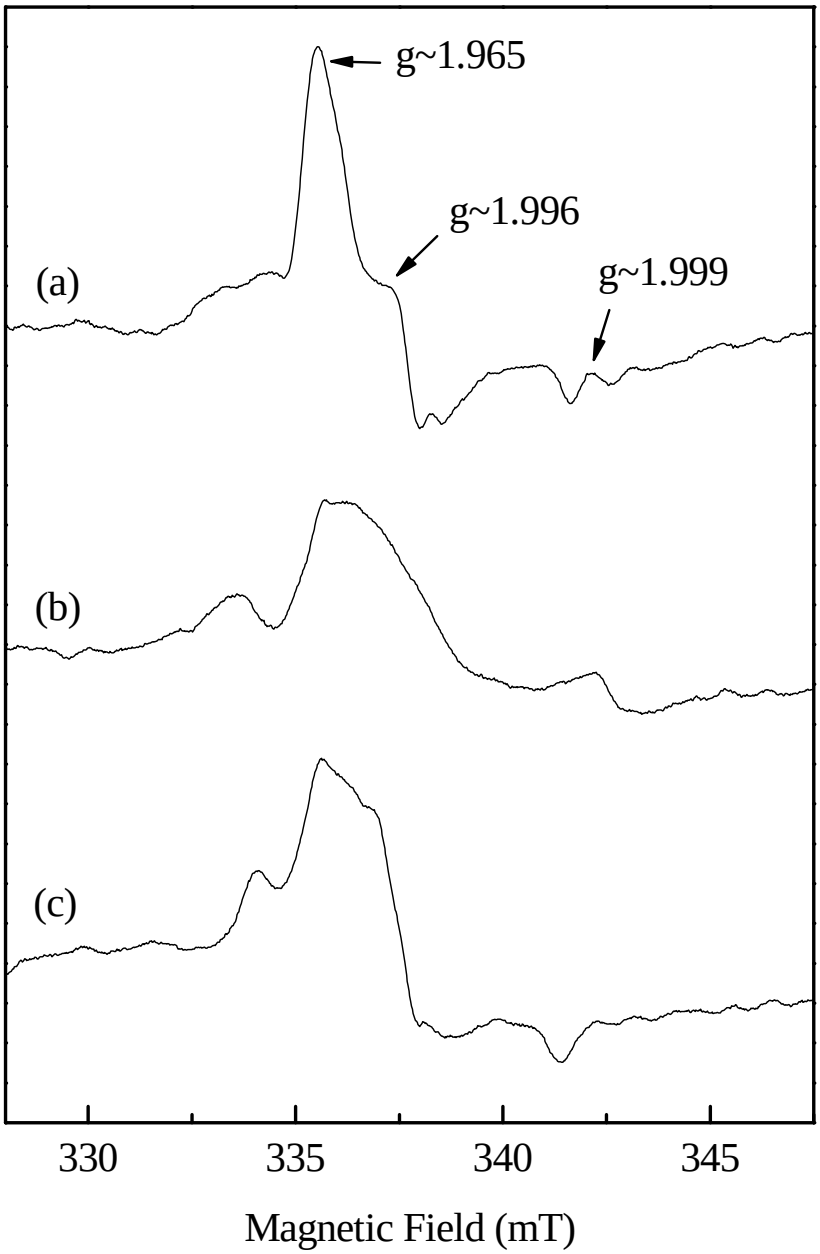

Biochemical Journal Immediate Publication. Published on 10 Aug 2007 as manuscript BJ20070669

Figure 9. Dridge *et al*.

A

MSQRQLAYVFDLNKCIGCHTCTMACKQLWTNRDGREYMYWNNVE
SRPGKGYPKNWEQKGGGFDKDGKLKTNGIIPIRADYGGTWNYNL
LETLVEGKSNQVVPDEKPTWGPNWDEDEGKGEFPNNHYFYLPRI
CNHCSNPACLAACPTKAIYKREEDGLVVVDQSRCKGYRYCVKAC
PYGKMYFNLQKGTSEKCIGCYPRVEKGEAPACVKQCSGRIRFWG
YRDDKDGPIYKLVDQWKVALPLHAEYGTEPNVFYVPPMNTTPPP
FEEDGRLGDKPRIPIEDLEALFGPGVKQALATLGGEMAKRRKAQ
ASELTDILIGYTNKDRYGI

B

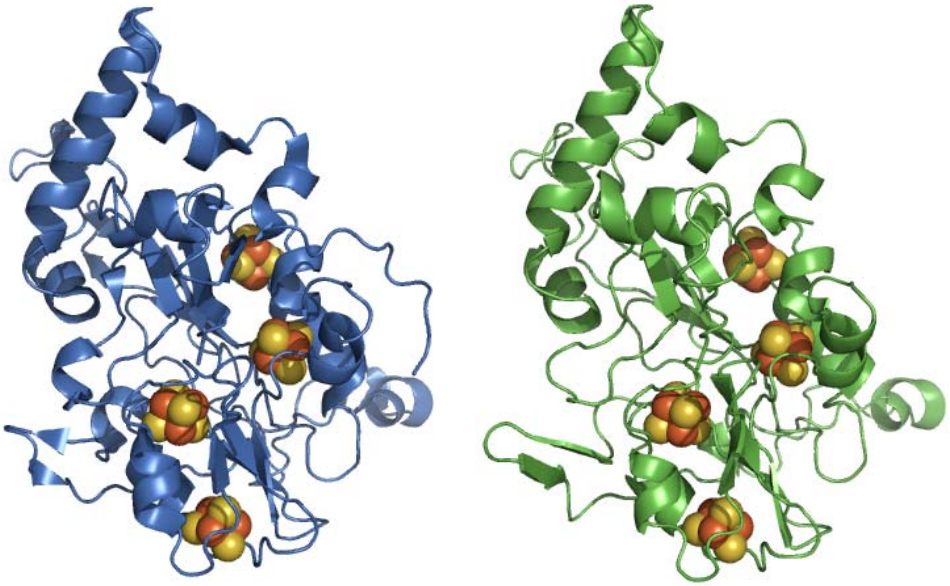

C

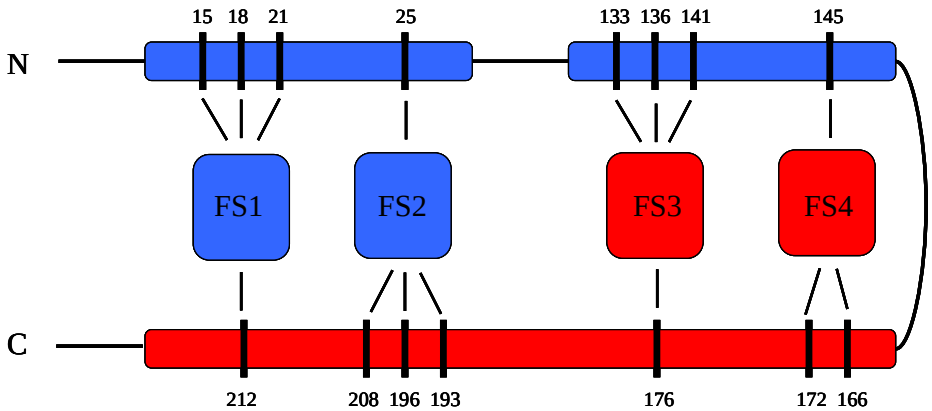

Biochemical Journal Immediate Publication. Published on 10 Aug 2007 as manuscript BJ20070669

Figure 10. Dridge *et al.*